Bayesian Analysis Reveals the Key to Extracting Pair Potentials from Neutron Scattering Data

Brennon L. Shanks, Harry W. Sullivan, and Michael P. Hoepfner*

Department of Chemical Engineering, University of Utah, Salt Lake City, UT, 84112, United States

E-mail: michael.hoepfner@utah.edu

Phone: +1 (801)-581-3504

Author Affiliations

1. Brennon L. Shanks: Department of Chemical Engineering, University of Utah, Salt Lake City, UT, 84112, United States

2. Harry W. Sullivan: Department of Chemical Engineering, University of Utah, Salt Lake City, UT, 84112, United States

3. Michael P. Hoepfner: Department of Chemical Engineering, University of Utah, Salt Lake City, UT, 84112, United States

Abstract

Learning interaction potentials from the structure factor is frequently seen as impractical due to accuracy constraints of neutron and X-ray scattering experiments. This study reexamines this historic inverse problem using Bayesian inference and probabilistic machine learning on a Mie fluid to elucidate how measurement noise impacts the accuracy of recovered potentials. To perform reliable potential reconstruction, we recommend that scattering data must have noise smaller than 0.005 up to ~ 30 Å^{-1} at a standard bin width 0.05 Å^{-1}. At uncertainties below this threshold, Mie potentials can be determined within approximately $\pm$ 1.3 for the repulsive exponent, $\pm$ 0.068 Å for atomic size, and $\pm$ 0.024 kcal/mol in well-depth with 95% confidence. These findings highlight the potential of uniting scattering and machine learning to overcome a century-old physics problem, infer local atomic forces to serve as a vital benchmark for model validation, and enhance the accuracy of molecular simulations.

TOC Graphic

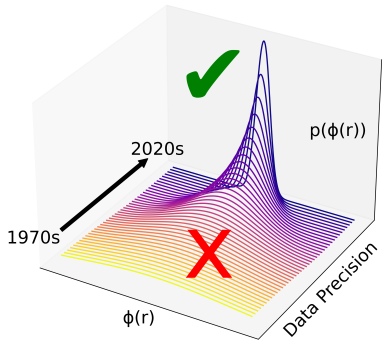

Reconstructing interatomic potentials from experimental scattering data is a historic inverse problem in statistical mechanics, motivated by the idea that complete knowledge of the effective interatomic potential with the atomic correlation functions allows for all thermodynamic properties of a classical liquid to be calculated.[1] While it has become widely accepted that liquid state systems exhibit significant many-body and quantum mechanical (both electronic and nuclear) interactions[2] that influence molecular dynamics, the fact that empirical molecular simulations remain the gold-standard for efficient and accurate liquid state materials modeling has maintained the significance and impact of the inverse problem in contemporary physics. However, despite over a century of research, with seminal works by Ornstein and Zernike,[3–5] Yvon, Born, and Green,[6] Schommer,[7] and Lyubartsev and Laaksonen,[8] there is surprisingly little to no evidence that these techniques can reliably extract force field parameters from experimental scattering data.[9] Furthermore, there is growing evidence that existing force fields provide inaccurate representations of fluid structure when compared to experimental estimates.[10,11] With the advent of state-of-the-art diffractometers and the rise of machine learning for robust uncertainty quantification (UQ), it is relevant to revisit and contextualize prior and current work to better understand how to resolve this longstanding challenge.

Serious attempts at determining the interatomic potential from experimental scattering data began in the 1950's. Henshaw (1958)[12] and later Clayton and Heaton (1961)[13] speculated that the ratio between the atomic collision radius and first solvation shell radius was related to the approximate width of the interatomic potential bowl. While this concept cannot directly extract the interatomic potential from the radial distribution function (RDF), it was used to conclude that argon and krypton could be reasonably represented by a (12-6) Lennard-Jones potential. Weeks, Chandler, and Anderson then introduced a separation of the pair potential into repulsive and attractive parts, in which they concluded that the repulsive part alone produces structure factors nearly identical to the repulsive and attractive parts taken together.[14] Henderson (1974) then proved that for a pairwise additive and homogeneous system with equal RDFs that the effective interatomic potential was unique up to an additive constant,[15] which was later implemented numerically by

Schommers (1983)[7] to study liquid gallium. Around the same time, Levesque (1985)[16] proposed a modified hypernetted chain closure to the Ornstein-Zernike integral relation to calculate interatomic potentials for liquid aluminum with fast convergence. Both studies were highly influential in the study of liquid metals, but offered little in resolving the inverse problem in general since interatomic potentials derived from these methods were only shown to accurately reproduce the diffusion coefficient and not other thermodynamic properties.

The most recent inverse methods applied to experimental data are Soper's (1996)[17] empirical potential structure refinement (EPSR) and Lyabartsuv and Laaksonen's (1995)[8,18,19] inverse Monte Carlo (IMC). EPSR is an iterative potential refinement method that is primarily used to determine real-space structures consistent with reciprocal space scattering data in fluid and glass systems. However, Soper's work on liquid water revealed that EPSR was not reliable at determining pair interaction potentials for molecular simulation applications.[20] On the other hand, IMC methods have been widely adopted for coarse-graining, in which the number of degrees-of-freedom of a molecular model are reduced by mapping atomic coordinates to "beads" of atom clusters. While both methods have attracted significant research interest in recent years, with the creation of an improved EPSR software package[21] and applications of IMC in complex biological systems[22] such as DNA[23] and nucleosomes,[24] the extraction of reliable and transferable interatomic potentials from experimental scattering data remains widely under-reported and unresolved, even for simple fluids such as noble gases.

We recently proposed structure-optimized potential refinement (SOPR)[25] as an alternative approach to extract pair potentials from scattering data (2022). SOPR is a probabilistic iterative Boltzmann inversion (IBI) algorithm that uses Gaussian process regression to address challenges such as numerical instability and over-fitting to uncertain experimental data. In this way, SOPR potentials are an experimental analogue to the widely used Gaussian approximation potential (GAP) approach.[26] SOPR derived potentials have demonstrated remarkable accuracy in the simultaneous prediction of both structural correlation functions and vapor-liquid equilibria of noble gases. Furthermore, the short-range repulsive decay rate determined with SOPR coincides with predictions

from an independently optimized ($\lambda - 6$) Mie force field for vapor-liquid equilibria.[27] This finding represents the most complete example of the inverse problem in real systems and highlights the potential of scattering data in studying both macroscopic thermophysical properties of liquids and improved accuracy of local structural predictions.

The transferability of SOPR potentials raises intriguing questions regarding what factors are most important to accurately extract local forces from scattering data. One possible explanation is that the reliability of structure inversion techniques hinges on data quality.[28] Levesque and Verlet (1968) speculated that experimental scattering error of $< 1\%$ was required to determine the interaction potential within an error of 10%,[29] but ultimately concluded that it is not possible to obtain quantitative information on the potential from scattering data due to systematic errors in the experiments. However, it is currently unclear to what extent these previous attempts have been impeded by experimental uncertainty. The reason for this knowledge gap is that rigorous uncertainty quantification and propagation (UQ/P) is computationally demanding and requires the use of machine learning surrogate models and advanced sampling methods[30–32] that were not available to liquid state theorists when these questions were first investigated. To test the hypothesis that neutron instrument accuracy is essential in force field extraction therefore lies at the crossroads of theoretical statistical physics, machine learning, and high-performance computing.

This study assesses how scattering measurement uncertainty impacts our ability to learn interatomic forces using a dataset of *in silico* experimental structure factors with varying levels of noise. Constant Gaussian noise was introduced to a reduced Mie model structure factor to represent neutron reactor source counting statistics[33] at a Q-space bin width of 0.05 Å^{-1}. The noise had standard deviation, δS, typical of the data quality accepted in the operating periods between 1973 and 2022 (Figure 1). Note that improvements in neutron flux associated with modern instruments serve to reduce the acquisition time for a given threshold of precision, and high-quality data could be generated on older instruments with longer duration experiments. Consequently, the constructed timeline serves as a general guide to the era's accepted standards rather than a strict measure of instrument improvement.

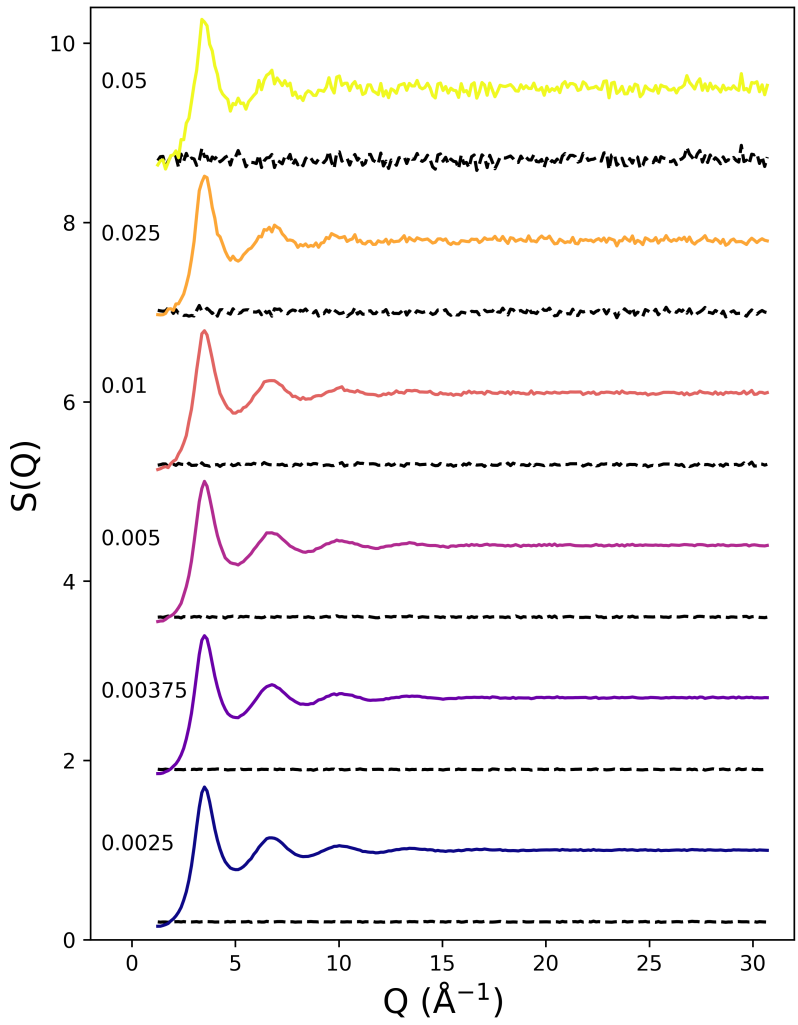

Figure 1: Static structure factors (colored lines) with introduced uncertainty (dotted black lines) for uniformly distributed noise. Measurement standard deviations δS are labeled to the left of the structure factor.

Accelerated Bayesian inference using a local Gaussian process (LGP) surrogate model was then applied to extract underlying probability distributions on the force field parameters. The LGP surrogate model, which mimics molecular simulation outputs at a 6 orders-of-magnitude reduction in computational cost,[32] provides a means to rigorously quantify how changes in each of the Mie parameters affect the structure factor via its analytical derivative with respect to the model

parameter, $\frac{\partial S(Q)}{\partial \theta}$. Figure 2(a) shows scaled derivatives, $\frac{\partial \tilde{S}}{\partial \theta} = \frac{\partial S(Q)}{\partial \theta} \max\left(\left|\frac{\partial S(Q)}{\partial \theta}\right|\right)^{-1}$, of the LGP structure factor given by the equation with respect to each parameter of the $(\lambda - 6)$ Mie force field. By visualizing these scaled derivatives, we gain insights into how variations in each of the Mie parameters affect the structure factor.

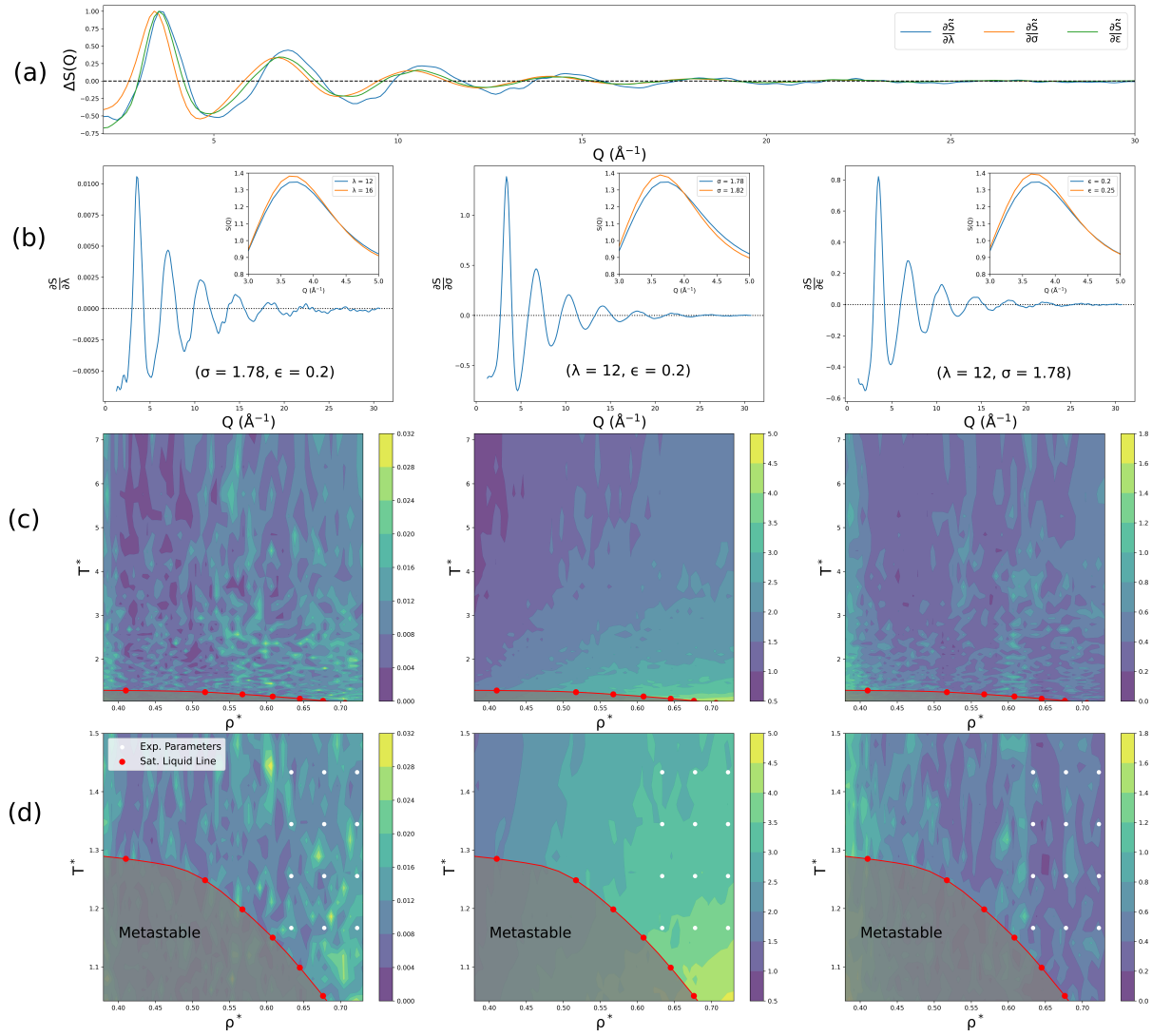

Figure 2: (a) Scaled LGP structure factor derivatives with respect to the Mie parameters at a reference of ($\lambda = 12$, $\sigma = 1.78$, $\varepsilon = 0.2$). (b) Examples of LGP structure factor derivatives with respect to the model parameters (λ, σ, ε) at the selected reference conditions. Inset figures show LGP predictions for the reference structure factor (blue line) and a modified structure factor (orange line) due to a perturbation in the parameter listed in the inset figure legend. (c) Heat map of the maximum absolute value of the structure factor derivative with respect to each parameter of the ($\lambda - 6$) Mie force field for the validated range of the surrogate model and (d) near the vapor-liquid coexistence line (red line). The grey region represents a metastable fluid that separates into vapor and liquid phases.

Notably, the derivatives for the repulsive exponent and the collision diameter are out of phase across all values of Q, highlighting that these aspects of the interatomic potential influence the structure factor in fundamentally distinct ways. As shown in Figure 2(b), the repulsive exponent

primarily sharpens or broadens the peaks and valleys of the structure factor without shifting their positions, whereas the collision diameter predominantly shifts peak positions in Q-space. Interestingly, the dispersion energy derivative closely tracks that of the repulsive exponent at the first peak before diverging to align with the collision diameter derivative, suggesting a non-linear influence of the potential tail on the structure. Overall, the distinct modifications to the structure factor by each parameter imply that Bayesian inference should be capable of differentiating their effects. Furthermore, as seen in the raw derivatives in Figure 2(b), the magnitude of the derivative for the repulsive exponent is significantly smaller (about 100 times) than those for atomic size and dispersive attraction, which quantitatively explains the difficulty in determining the repulsive exponent from structural data. However, the persistence of non-zero derivative values for the repulsive exponent at high Q suggests that high-resolution scattering data extending to high Q_{max} could potentially distinguish between different repulsive exponents.

Computation of the LGP derivative can also be performed over the entire validated range of the surrogate model. To visualize the results, we present a heat map of the maximum of the absolute value of the derivative, $\max\left(\left|\frac{\partial S(Q)}{\partial \theta}\right|\right)$ with respect to reduced temperature $T^* = T/\varepsilon$ and reduced density $\rho^* = \rho\sigma^3$ in Figure 2 (c). Yellow regions indicate a high sensitivity of the structure factor relative to the lower sensitivity blue regions. First note that the maximum derivative estimates vary in magnitude significantly, with a two orders-of-magnitude smaller value for the repulsive exponent (0.04) compared to the collision diameter (5.0) and dispersion energy (1.35). The repulsive exponent λ exhibits biomodality as a function of ρ^*, with higher sensitivity regions tending towards higher densities. The structural sensitivity at high density could be explained by the fact that such systems tend to collide more frequently at close range which is where the repulsive exponent strongly influences the potential energy function. The collision diameter σ has a clear trend with more sensitive regions being higher density and lower temperature.

We can see that there also appears to be asymptotic behavior near specific densities, suggesting that higher sensitivities correspond to closer proximity of the atoms where excluded volume effects can dominate the structure. This finding is fully consistent with Weeks, Chandler, and Anderson's

conclusion that there is a shift in structural sensitivity near a reduced density of $\rho^* = 0.5$.[14] Finally, the dispersive forces appear to become more significant to the structure near and above the critical temperature and at high density and temperatures. An avenue of further investigation on pair potential sensitivity may show that there is a relationship between the potential and supercritical transitions, such as the Frenkel,[34] Widom,[35] or Fisher-Widom lines.[36] However, to thoroughly explore trends and patterns in structural sensitivity to the interaction potential, an LGP surrogate model would need to be trained across a broader range of the Mie fluid phase diagram.

Armed with a precise and fast surrogate model for the Mie fluid structure factor, we can now proceed to evaluate the likelihood and, consequently, estimate Bayesian posterior distributions. By studying these posterior probability distributions as a function of introduced uncertainty, we aimed to challenge the assertion that structure factors are insensitive to the detailed form of interatomic interactions.[37] Indeed, the Bayesian inference directly quantifies how interatomic interactions such as short-range repulsion, excluded volume, and dispersion energy affect the structure factor, shedding light on the intricate relationship between pair potentials and structural features. Surprisingly, we find that the conclusions from prior literature stating that details of the interatomic interaction could not be extracted from experimental structure factors were likely justified given the data quality available at the time, but that modern neutron instruments exceed a precision threshold where this conclusion could be overturned. These findings suggest that experimental inverse techniques were prematurely abandoned by the molecular modeling community and should be revisited.

Figure 3 illustrates experiment averaged marginal probability distributions of $(\lambda, \sigma, \varepsilon)$ as a function of noise. The 1D Marginal distributions in Figure 3 are obtained by integrating the joint posterior probability distribution over all but one model parameter. The mode of the marginal distribution corresponds to the marginal *maximum a posteriori* (*MAP*). Clearly, as the uncertainty in the structure factor increases the marginal distributions become wider and flatter. This behavior is expected, as greater uncertainty in the observation leads to increased uncertainty in the parameter distribution. Notably, in cases where the structure factors exhibit low uncertainty the *MAP* estimates accurately recover the unknown force field parameters. Deviation between the *MAP* estimate

and true parameter value is tabulated as a function of uncertainty and reported in the Supporting Information.

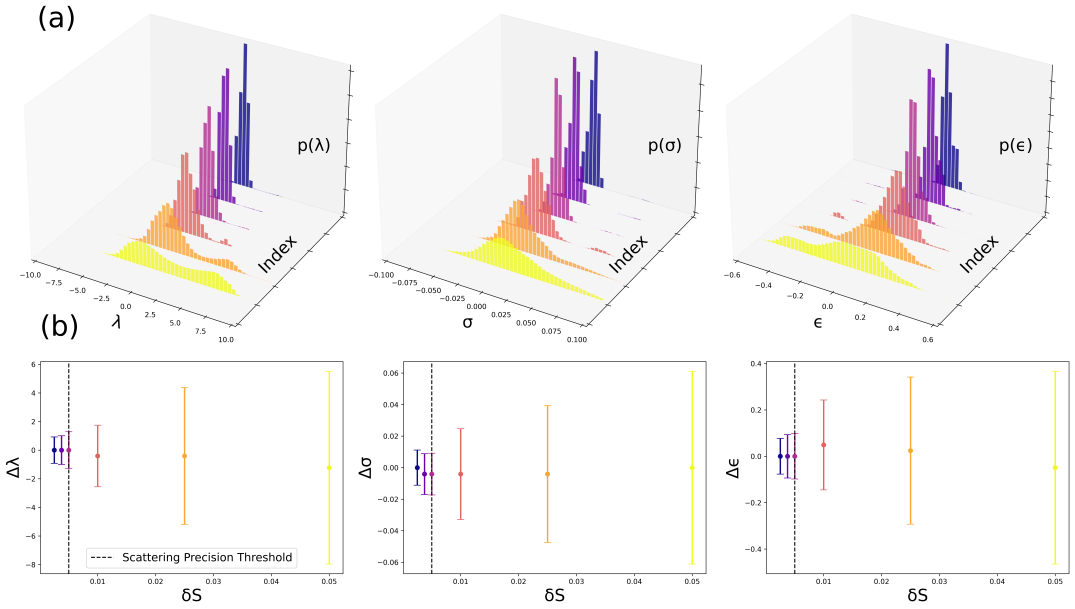

Figure 3: Average marginal distributions computed from the 16 reference posterior distributions. (a) Histograms of the average marginal distributions on the $(\lambda - 6)$ Mie force field parameters as a function of uncertainty in the structure factor (δS). (b) MAP estimates (points) are plotted with 2 std. dev. error bars as a function of noise. Low parameter uncertainty cases (blue) are compared to high uncertainty cases (red) and the lower limit precision of current neutron instruments (black dashed line). Low and high uncertainty distributions were separated based on the near doubling of the standard deviation between $\delta S = 0.005$ and $\delta S = 0.01$.

First, note the drastic difference in the accuracy of the *MAP* estimates for the repulsive exponent and dispersion energy parameters as we transition from an uncertainty level of $\delta S = 0.025$ to $\delta S = 0.05$, indicating a significant loss in information between these two noise levels. However, the σ parameter is accurately estimated regardless, demonstrating its reliable prediction even for low quality scattering data. In the $\delta S = 0.025$ case, the λ and ε parameters are also accurately predicted. However, for the $\delta S = 0.05$ case, learning the λ and ε parameters becomes unreliable with *MAP* deviations of -1.173 and -0.05, respectively.

The data also shows a significant change in the width of the distributions at critical uncertainty levels. The standard deviation effectively doubles for the Mie parameters between $\delta S = 0.005$ and $\delta S = 0.01$. This rapid increase in width of the posterior distribution is significant since it

becomes exceedingly more difficult to estimate the potential parameters using optimization techniques. Based on these shifts in the standard deviations, we recommend that scattering experiments for liquids not exceed random errors of $\delta S = 0.005$ to ~ 30 Å^{-1} at Q-space bin width of 0.05 Å^{-1} if attempting to extract pair potential information from the structure factor. Fortunately, this level of precision is already available at modern diffractometers, such as the Nanoscale Ordered MAterials Diffractometer (NOMAD)[38] or at other modern instruments for sufficiently long run times. Method advancements in structure inversion, along with the improvement of neutron facilities and measurement accuracy, may therefore be the key to unlock a wealth of new opportunities for improving molecular models, characterizing local atomic forces, and understanding the dynamics of atoms and molecules in relation to complex and emergent physical phenomena.

These observations are critical to contextualize prior studies in which it has been concluded that the structure factor is insensitive to the interatomic interactions beyond the excluded volume[2,37] or that uncertainty in the structure measurement impeded prediction of transferable potentials.[7,8,16] In these studies, structural uncertainty ranged from values of 0.03-0.07, exceeding the precision threshold identified by our model.

In a nutshell, we have demonstrated that prior attempts at estimating interatomic potentials from structure factors were likely thwarted by high uncertainty present in experimental scattering measurements. As we have shown, noise in structure factor data can significantly impact the broadness of parameter probability distributions, compromising the effectiveness of optimization methods to accurately estimate the parameter *MAP*. However, we also contend that modern neutron diffraction sources have recently crossed a critical precision threshold, enabling reliable inverse problem solutions to assess a variety of interatomic properties.

So then, how precisely should we expect to recover interatomic force parameters from such data? An estimation of these credibility intervals can be gleaned from the parameter posterior distributions for structure factor results consistent with modern diffractometers. To this aim, we studied the posterior distribution of structure factors with constant standard deviations of $\delta S =$ 0.005 out to 30 Å^{-1}, which well-represents an uncertainty upper bound for modern spallation

sources such as NOMAD and NIMROD. Posterior marginals, MCMC samples, and heat maps of the joint posterior distribution for this case are presented in Figure 4.

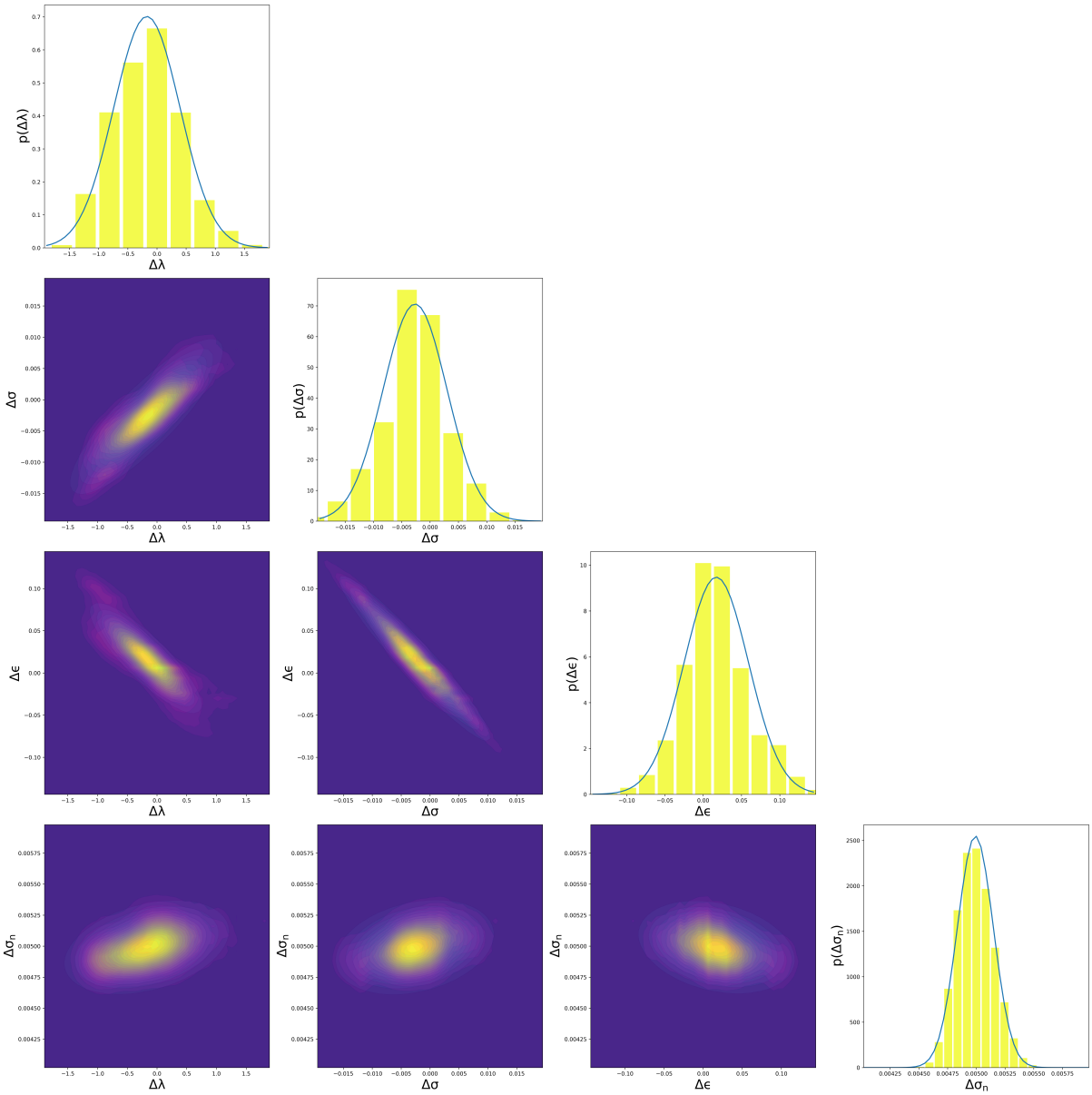

Figure 4: Marginal distributions on the $(\lambda - 6)$ Mie force field parameters for $\delta S = 0.005$ at 30 $\mathring{A}^{-1}$ with variance sampled with MCMC plotted with known parameter values.

The marginal *MAP*, corresponding to the global maximum of the marginal distribution, accurately predicts the true parameter values (indicated by red dashed lines) with exceptional precision, exhibiting error rates below 1% for all force parameters. Furthermore, the shape and width of the marginal distributions offer valuable insights into the influence of each parameter on the ensemble

fluid structure. The collision diameter marginal exhibits a narrow and symmetric shape, characterized by a probability density at the *MAP* that surpasses the repulsive exponent and dispersion energy by factors of 80 and 3, respectively. This symmetry and high probability density suggest a remarkable sensitivity of the structure factor to changes in the effective particle size, consistent with the observations of Weeks, Chandler and Anderson.[14] However, the seemingly small difference between the repulsive structure factor alone and the true structure factor clearly contains sufficient information to determine the potential well-depth as well as the repulsive exponent and collision diameter. Therefore, we contend that the structure factor of liquids contains more information than previously believed.

Two standard deviations of the posterior distribution can be used as an estimate of our confidence in recovering the force parameter from the structure factor. Using this metric, we find that the force parameters can be recovered with 95% confidence within ± 1.3 for the repulsive exponent, ± 0.02 σ, and ± 0.1 ε. Of course, the posterior distributions computed here are in reduced Lennard-Jones (LJ) units and must be scaled by a known reference to approximate the credibility intervals in real units. For example, taking the LJ parameters for argon ($\sigma = 3.4$ Å, $\varepsilon = 0.24$ kcal/mol[25]) would give a real unit estimate of $\lambda \pm 1.3$, $\sigma \pm 0.068$ Å, and $\varepsilon \pm 0.024$ kcal/mol.

UQ on the potential parameters in relation to the structure factor holds the key to unlocking several novel capabilities of neutron scattering, including force field design, elucidation of many-body interactions, and improved understanding of structural properties in fluid systems.[39] While these aims have motivated research on the inverse problem for over a century, we are only now seeing evidence that accurate structure inversion on experimental data is possible. We argue that our results warrant the re-visitation of structural inverse methods for liquid state modeling.

However, many questions regarding UQ/P for experimental scattering data remain unresolved. For example, the noise in the structure factor is directly influenced by the number of neutron counts per bin, which is highly sensitive to the experimentalist's choice of Q-space bin width. In this study, we fixed the bin width at a typical value of 0.05 Å^{-1}, so that the structure factor noise represents the uncertainty in neutron counts / 0.05 Å^{-1}. Due to the computational burden

of retraining the LGP surrogate model and re-computing the posterior distributions, we did not investigate how varying the bin width affects the results. We hypothesize that the trade-offs inherent in the Bayesian posterior equation would likely mitigate the impact of varying the bin width on the results given a fixed number of neutron events. Specifically, increasing the bin width reduces noise by aggregating more counts per bin but simultaneously decreases the number of observations available to inform the likelihood. This balance should, in principle, lead to posterior distributions that are relatively insensitive to bin width changes. Ideally, the binning should align with the precise resolution of the instrument to fully exploit UQ on the collected data. Nevertheless, it remains an open question whether artificially increasing the Q-space bin width for data with fewer neutron counts (i.e., shorter instrument run times) could achieve sufficient statistical precision for learning potentials.

Another unresolved question is how noise in the structure factor propagates to its r-space counterpart, the RDF. Since the RDF is not directly observed, uncertainties in the neutron counts must be propagated into r-space through the radial Fourier transform. This Fourier dual relationship between the structure factor and RDF means that the uncertainty in the real space representation is non-trivially dependent on the uncertainty in the momentum space. A rigorous approach to address this problem could involve applying non-stationary Gaussian process regression (NS-GPR) to the experimental scattering data. Non-stationary refers to functions in which the mean and covariances change as a function of input, as is the case for an RDF which has known limiting behaviors (i.e., $\lim_{r\to 0} g(r) = 0$ and $\lim_{r\to\infty} g(r) = 1$). Using this expert knowledge, it is possible to construct a non-stationary mean and covariance function in real space for the RDF and inverse Fourier transform them to obtain a Fourier dual mean and covariance in momentum space. Then, by performing regression over the observed momentum space data and radial Fourier transforming the resulting NS-GPR posterior, an r-space GP posterior is obtained that estimates the likely distribution of RDFs given the experimental observations. While this approach is outside the scope of the current study, it presents an intriguing direction for future research.

An exciting application for the structural inverse problem in general is using structure-derived

interaction potentials as an external validation to computationally expensive bottom-up atomistic models. One example is electron structure calculations, in which a highly accurate quantum mechanical treatment of the electron structure can reveal insights into potential energy surfaces and reaction mechanisms. Electron structure methods have become faster and more robust due to quantum computing,[40] clever basis set selection,[41] and machine learning.[42,43] However, as these more fundamental theories of atomic structure and motion become commonplace, experimental neutron scattering data will become increasingly crucial to validate their predictions. Indeed, we have already shown that many-body interactions in noble gases are consistent with electron structure calculations in trimeric systems.[25,44] Further advancement of inverse methods can provide quantifiable validation of many-body interactions in progressively complex systems.

In addition to experimental data analysis, structure inversion methods have been widely used in contemporary chemical physics for for coarse-graining,[45–49] in which all atom systems are mapped onto a reduced coordinate space of "beads" to improve computational speed. In coarse-graining, structure factors (or more commonly the partial RDFs) are generated from a known model where structural uncertainty fluctuations are significantly smaller than that of experimental data. In such cases, our results suggest the presence of global maxima within narrow posterior distributions, which may explain the success of traditional optimization techniques in recovering coarse-grained force field parameters from all-atom simulations. Moreover, since a well-behaved parameter space is also evident in highly precise, state-of-the-art experiments, there is a promising opportunity to leverage existing coarse-graining methods for experimental scattering analysis. As a result, we believe the connection between experimental and simulation-based structure inversion techniques is becoming clearer and could lead to significant breakthroughs in the near future.

Finally, it is important to acknowledge the limitations of generalizing these results to broader systems. First, the sensitivity of complex systems to variations in the potential may differ from those observed in the Mie fluid model, so our findings should be viewed as a conceptual exploration of how classical two-body interactions shape atomic organization in fluids. Hence, we stress that the specific response of complex systems to variations in interatomic forces should be studied

individually. Second, if a fluid is not well-described by the (λ-6) Mie model, reliable recovery of force parameters cannot be guaranteed, and a more accurate model may be necessary. Third, we did not account for systematic errors arising from inelastic or multiple scattering subtraction, nor from variations in Q-space binning. These considerations are particularly important for extending our conclusions to X-ray scattering data, where the treatment of scattering corrections and binning methodologies can differ significantly. Nonetheless, the accuracy threshold established in this study remains directly applicable to X-ray scattering data, provided that appropriate form factors and scattering corrections are incorporated to mitigate the introduction of additional errors. Addressing systematic errors and rigorously quantifying their associated uncertainties are therefore essential to achieving the level of precision required for reliably extracting interaction potentials from scattering data.

Conclusions

Rigorous uncertainty quantification and propagation analysis has shown that modern neutron diffractometers have attained the necessary accuracy for reliable force field reconstruction. It has also been shown that measurements within ≤ 0.005 at $\sim$30 Å^{-1} are likely sufficient for force parameter recovery in Mie-type fluids. We emphasize that the structure factor (1) encapsulates information on both the attractive and repulsive components of the interatomic potential, and (2) that the commonly held opposing view likely emerged due to the poor quality of scattering data available during the early, pivotal stages of liquid modeling research. This study highlights the exciting possibility of using neutron scattering to predict the potential energy function, emphasizes the critical role of experimental precision in extracting potentials from scattering data, and offers valuable insights into the nature of interatomic forces in liquids.

Finally, the significance of this work extends beyond the field of neutron scattering. The results indicate significant potential for advancing force field design and optimization, enabling the development of more effective coarse-graining techniques, and facilitating the exploration of many-body

effects in fluid ensembles. In summary, this research highlights the transformative potential of machine learning in extracting interatomic forces from experimental structure measurements within a rigorous UQ framework.

Theory and Computational Methods

In this study, we modeled how uncertainty propagates from neutron scattering data to the estimation of force field parameters. The impact of measurement uncertainty was isolated by constraining the Bayesian analysis to a classical model fluid. While real physical systems behave quantum mechanically and are inherently many-body in nature, classical pairwise additive model fluids continue to be studied due their low computational cost and accurate predictions of complex thermodynamic properties. Furthermore, our prior work has shown that SOPR potentials exhibit potential corrections consistent with quantum mechanical calculations,[25] suggesting that effective pair interactions could be found that capture many-body and quantum mechanical contributions.

The (λ-6) Mie fluid model was selected since it is a flexible and widely successful classical model with numerous existing and developing applications for materials modeling.[27,50] The pairwise, non-bonded potential energy term of the (λ-6) Mie fluid is,

$$v_2^{Mie}(r) = \frac{\lambda}{\lambda - 6}\left(\frac{\lambda}{6}\right)^{\frac{6}{\lambda-6}} \varepsilon \left[\left(\frac{\sigma}{r}\right)^{\lambda} - \left(\frac{\sigma}{r}\right)^{6}\right] \tag{1}$$

where λ is the short-range repulsion exponent, σ is the collision diameter (distance), and ε is the dispersion energy (energy).[51]

Modeling Neutron Measurement Uncertainty in a Mie Fluid Model

To model experimental uncertainty, a set of Mie fluids was simulated with sufficient sampling statistics to calculate a highly-accurate static structure factor ($\delta S(Q) < 0.001$) to $Q_{max} = \sim 30$ Å^{-1}) with Q-space bin width of 0.05 Å^{-1}. Computer generated atomic trajectories were calculated in HOOMD-Blue.[52] MD simulations were initiated with a random configuration of 500 particles at

reduced density $\rho^* = 0.1$ and reduced temperature $T^* = 1$ and equilibrated with Langevin dynamics for 1×10^5 timesteps ($dt = 10$ femtoseconds). Potentials were truncated at 3σ with an analytical tail correction, and RDFs were calculated with Freud.[53] Static structure factors are calculated via radial Fourier transform of the RDF.

Experimental measurements of structure factors are subject to uncertainty arising from various factors, including experimental, model, and numerical sources. Uncertainties in neutron flux, energy, time-of-flight, minimum and maximum momentum transfer (Q_{min}, Q_{max}), and data collection time contribute to uncertainty in neutron counting statistics and the effective resolution of the instrument. Post-processing corrections for inelastic, incoherent, multiple, and low momentum transfer scattering further contribute to uncertainty in the structure factor form.[54] These effects result in variations in the neutron intensity that are not necessarily normally distributed;[55] however, errors from neutron detection are normal due to the limiting behavior of the Poisson distribution for large number of counts.[56] For reactor source instruments, the variance due to these random errors remains approximately constant to a limited Q-max (10-20 Å^{-1}), while for spallation sources, the variance increases proportionally to the square of the momentum transfer to a higher Q-max of 50-125 Å^{-1}.[38] Currently, the extent to which this uncertainty influences the accuracy and reliability of force field reconstructions remains unknown.

UQ was performed for reactor type neutron instruments by adding Gaussian noise with standard deviations equal to twice the values of those indicated in Figure 1 to four replicates of the simulated structure factor. Using multiple replicates of the noisy structure factor as a data target reduces the chance of over fitting to a single, randomly generated structure factor. Of course, this modeling approach is not directly consistent with an actual scattering measurement which is typically reported as a single measurement over a fixed length of time. However, it is well-known that the standard deviation in neutron counting statistics is proportional to the square-root of the number of counts.[56] Assuming that neutron counts are equally distributed over the course of a measurement, we then expect that four structure factor replicates with twice the standard deviation of the target structure factor is approximately equivalent to the single target scattering pattern.

Bayesian analysis was then performed over 16 *in silico* experimental conditions on a 4×4 equal spaced grid in the reduced Mie diagram (σ, ε) where $\sigma = [1.85, 1.89, 1.93, 1.97]$, $\varepsilon = [0.86, 0.80, 0.74, 0.70]$ and fixed $\lambda = 12$. Since spallation type neutron instruments have a Q^2-dependent random error, UQ on the constant error can be interpreted as an uncertainty upper bound for spallation type instruments up to a given Q. For instance, if statistical noise of a spallation source measurement is 0.025 at 30 Å^{-1}, then we would expect the noise to be smaller down to an appropriately selected $Q_{min} < Q < 30$ Å^{-1}. Uncertainty levels were selected based on published data of structure factors measured on neutron instruments from the early 1970's to 2022. Notably, a classic argon data set collected at the Omega West reactor (1973)[57] is well approximated by constant noise with variations in $S(Q)$ of approximately $\delta S = 0.05$, as noted in Figure 1. Similarly, krypton data collected on D4B (1993)[58] is approximated by the constant $\delta S = 0.025$ case, while modern instruments such as NOMAD and NIMROD (>2010) regularly achieve uncertainty distributions similar to the $\delta S = 0.005 - 0.01$ cases depending on the data collection time.[38,59] Two low uncertainty extremes were chosen beyond these reported values to identify measurement precision thresholds and model trends in the predictability of force parameters.

Bayesian Uncertainty Quantification for Force Field Reconstruction

According to the Henderson inverse theorem, it is theoretically possible to uniquely recover the underlying potential in a pairwise additive, homogeneous fluid.[15] In the context of Bayesian optimization, Henderson's theorem requires that there should be a global maximum in the posterior probability distribution at the unique force parameters. However, as the uncertainty in the structure factor signal increases, deviations from this unique potential are expected, causing the probability distributions to broaden. This broadening indicates a decrease in confidence in the estimation of the model parameters. In other words, as structural uncertainty increases, our ability to accurately predict the potential energy decreases, leading to a wider range of possible parameter values to explain the data.

Bayesian inference was implemented to calculate parameter probability distributions as a func-

tion of structure factor uncertainty. For simplicity of notation, let $\boldsymbol{\theta} = \{\lambda, \sigma, \varepsilon, \sigma_n\}$ represent the model parameters and $\mathscr{Y} = S_d(Q)$ be the structure factor observations. The nuisance parameter, σ_n, represents the width of the Gaussian likelihood and captures uncertainty from the experimental data and Gaussian process model, which is not known *a priori*. Calculating the posterior probability distribution with Bayesian inference then requires two components: (1) prescription of prior distributions on the model parameters, $p(\boldsymbol{\theta})$, and (2) evaluation of the structure factor likelihood, $p(\mathscr{Y}|\boldsymbol{\theta})$. The prior distribution over the $(\lambda - 6)$ Mie parameters is assumed to be a multivariate log-normal distribution,

$$\theta - \gamma_\theta \sim \log \mathscr{N}(\mu_\theta + \gamma_\theta, \sigma_\theta^2) \tag{2}$$

where μ_θ and σ_θ^2 are the prior mean and variance of each parameter in $\boldsymbol{\theta}$ and $\gamma_\theta \in \mathbb{R}$ is a real-valued parameter shift that enforces a lower bound. A wide, shifted multivariate log-normal distribution was selected because it is non-informative and imposes non-negativity constraints on the model parameters. Specifically, $\lambda - 6$ (defined by the Mie type fluid), σ, ε, and σ_n must be positive. For reference, the prior parameters used in this study are provided in the Supporting Information.

The likelihood function is known to be a Poisson distribution of neutron counts, but in the high count limit (which is effectively achieved in a neutron experiment) it approaches a Gaussian distribution,

$$p(\mathscr{Y}|\boldsymbol{\theta}) = \left(\frac{1}{\sqrt{2\pi}\sigma_n}\right)^{\eta} \exp\left[-\frac{1}{2\sigma_n^2}\sum_j \left[S_{\boldsymbol{\theta}_i}(Q_j) - S_d(Q_j)\right]^2\right] \tag{3}$$

where $S_{\boldsymbol{\theta}}(Q_i)$ is the molecular simulation predicted structure factor, η is the number of observed points in the structure factor, and j indexes over these points along the momentum vector. Bayes' theorem is then expressed as,

$$p(\boldsymbol{\theta}|\mathscr{Y}) \propto p(\mathscr{Y}|\boldsymbol{\theta})p(\boldsymbol{\theta}) \tag{4}$$

where equivalence holds up to proportionality. This construction is acceptable since the resulting

posterior distribution can be normalized *post hoc* to find a valid probability distribution. For further details see the following excellent reviews of Bayesian inference.[60,61]

The Bayesian likelihood distribution is estimated using Markov Chain Monte Carlo (MCMC) samples over the model parameters $\theta = \{\lambda, \sigma, \varepsilon, \sigma_n\}$. Computationally, a sample of the model parameters is drawn from a Metropolis-Hastings type algorithm, passed to the surrogate model, evaluated, and compared to the *in silico* structure factor. MCMC samples were calculated using the emcee package[62] from 160 walkers with dynamic burn-in and sample time based on the autocorrelation convergence criterion used in the emcee package and default stretch move with dynamic tuning.

After the posterior distributions were computed for all experimental conditions and uncertainty levels, the marginal posterior histograms were averaged over all experimental conditions. Histogram averaging was performed by defining a fixed range and bin count for all posterior marginals and weighting the distribution counts by the ratio of the number of counts for a given experiment with the total number of counts over all experiments. In other words, if $p_{a,b}(\theta)$ is the marginal posterior probability distribution for experiment condition a, uncertainty b, on model parameter θ, then the average marginal posterior $\mathscr{P}_b(\theta)$ for uncertainty level b is given by,

$$\mathscr{P}_b(\theta) \approx \sum_a \frac{n_{a,b}}{\sum_a n_{a,b}} p_{a,b}(\theta) \tag{5}$$

where $n_{a,b}$ is the number of independent MCMC samples for experiment a and uncertainty b. Conceptually, these average marginal posteriors are an approximation to the marginal parameter posterior distributions over the joint probability density containing the model parameters, structure factor, and thermodynamic state, $p(\lambda, \sigma, \varepsilon, S(Q), T^*, \rho^*)$, where $T^* = k_b T/\varepsilon$ and $\rho^* = \rho\sigma^3$ are the reduced temperature and density, respectively. More rigorous approximations derived from methods such as Gibbs sampling were not implemented due to the extremely high computational cost per experiment.

Local Gaussian Process Surrogate Models for Structure Factors

The process of populating the posterior distribution function necessitates the evaluation of likelihood for each condition of interest within the model parameter space, which, in turn, requires conducting an infeasible number of molecular dynamics simulations. The computational burden associated with this procedure renders the Bayesian framework impractical even for a relatively small number of samples. To illustrate this, consider the task of obtaining a collision diameter posterior distribution with a grid resolution of approximately 2% across a wide prior range of m_σ (ranging from 0.5 to 1.5). Achieving such resolution for just the m_σ parameter alone would demand a minimum of 50 samples. If the same level of resolution is desired for the remaining two parameters, a staggering 125,000 molecular simulations are required to comprehensively quantify the posterior distribution space. Clearly, there is a substantial computational challenge involved in obtaining accurate and comprehensive posterior distributions within the Bayesian framework.

To expedite the evaluation of the Bayesian likelihood, a local Gaussian process (LGP) surrogate model[32] was trained to generate structure factors based on a training set of 960 randomly sampled (λ-6) Mie parameters in a prior range specified in the Supporting Information. This range of parameters was selected to correspond with the liquid phase region of the Mie phase diagram and avoid pathological simulations that can occur near phase transitions. Note that this range will change based on the arbitrary choice of temperature and density for the Mie fluid simulation; but, since the reduced phase diagram is simply scaled from these values, the molecular dynamics simulation will have the same dynamics, average thermodynamic properties and structure.

LGP surrogate models reduce the computational time complexity of standard GP regression without compromising predictive accuracy.[63–65] Hyperparameter selection was performed using Bayesian optimization with Markov chain Monte Carlo and surrogate model accuracy was determined to have a root-mean-square error (RMSE) of 0.0036 for a 160 randomly sampled test set within the surrogate parameter range. Surrogate model validation and hyperparameter training is discussed further in the Supporting Information.

Data Availability

The datasets generated during and/or analysed during the current study are available from the corresponding author on reasonable request. Python codes for data generation and analysis are provided on GitHub at https://github.com/hoepfnergroup/Bayesian-Neutron-Potentials.

Acknowledgements

This study is supported by the National Science Foundation Award No. CBET-1847340. The support and resources from the Center for High Performance Computing at the University of Utah are gratefully acknowledged.

Author Contributions

B.L.S contributed towards conceptualization, algorithm development and implementation, data visualization, and writing. H.W.S provided contributions to conceptualization, algorithm development, and implementation. M.P.H contributed to conceptualization, funding acquisition, and manuscript revision and preparation.

Competing Interest

The authors declare no conflicts or competing interests.

Supporting Information Available

The following files are available free of charge as supporting information for the results presented in this manuscript. To promote reproducibility, all the code and data files required to reproduce the results of this manuscript are provided on GitHub.

- si.pdf: Details of the Bayesian model/priors (Table S1), local Gaussian process surrogate model training (Table S2-LGP training range, Figure S1-hyperparameter posterior) and validation (Table S3-parameter range for LGP validation, Figure S2-root mean square error over test set), and tabulated data for the Bayesian marginal distributions from Figure 3 (Table S4).
- GitHub: https://github.com/hoepfnergroup/Bayesian-Neutron-Potentials

References

(1) Kirkwood, J. G.; Buff, F. P. The statistical mechanical theory of solutions. I. *J. Chem. Phys.* **1951**, *19*, 774–777.

(2) Hansen, J.; McDonald, I. R. *Theory of Simple Liquids: With Applications to Soft Matter*; Academic Press, 2013.

(3) Ornstein, L. S.; Zernike, F. Accidental deviations of density and opalescence at the critical point of a single substance. *Proc. Acad. Sci. Amsterdam.* **1914**, *17 II*, 793–806.

(4) Percus, J. K.; Yevick, G. J. Analysis of classical statistical mechanics by means of collective coordinates. *Phys. Rev.* **1958**, *110*, 1–13.

(5) Percus, J. K. Approximation methods in classical statistical mechanics. *Phys. Rev. Lett.* **1962**, *8*, 462–463.

(6) Born, M.; Green, H. S. A kinetic theory of liquids. *Nature* **1947**, *159*, 251–254.

(7) Schommers, W. Pair potentials in disordered many-particle systems: A study for liquid gallium. *Phys. Rev. A* **1983**, *28*, 3599–3605.

(8) Lyubartsev, A. P.; Laaksonen, A. Calculation of effective interaction potentials from radial distribution functions: A reverse Monte Carlo approach. *Phys. Rev. E* **1995**, *52*, 3730–3737.

(9) Tóth, G. Interactions from diffraction data: historical and comprehensive overview of simulation assisted methods. *J. Phys. Condens. Matter* **2007**, *19*, 335220.

(10) Amann-Winkel, K.; Bellissent-Funel, M.-C.; Bove, L. E.; Loerting, T.; Nilsson, A.; Paciaroni, A.; Schlesinger, D.; Skinner, L. X-ray and Neutron Scattering of Water. *Chemical Reviews* **2016**, *116*, 7570–7589, Publisher: American Chemical Society.

(11) F. Headen, T.; L. Cullen, P.; Patel, R.; Taylor, A.; T. Skipper, N. The structures of liquid pyridine and naphthalene: The effects of heteroatoms and core size on aromatic interactions. *Phys. Chem. Chem. Phys.* **2018**, *20*, 2704–2715.

(12) Henshaw, D. G. Atomic distribution in liquid and solid neon and solid argon by neutron diffraction. *Physical Review* **1958**, *111*, 1470–1475.

(13) Clayton, G. T.; Heaton, L. Neutron diffraction study of krypton in the liquid state. *Phys. Rev.* **1961**, *121*, 649–653.

(14) Weeks, J. D.; Chandler, D.; Andersen, H. C. Role of repulsive forces in determining the equilibrium structure of simple liquids. *J. Chem. Phys.* **1971**, *54*, 5237–5247.

(15) Henderson, R. L. A uniqueness theorem for fluid pair correlation functions. *Phys. Lett. A* **1974**, *49*, 197–198.

(16) Levesque, D.; Weis, J. J.; Reatto, L. Pair interaction from structural data for dense classical liquids. *Phys. Rev. Lett.* **1985**, *54*, 451–454.

(17) Soper, A. K. Empirical potential Monte Carlo simulation of fluid structure. *Chem. Phys.* **1996**, *202*, 295–306.

(18) Tóth, G. Determination of pair-potential parameters from experimental structure factors. *J. Chem. Phys.* **2001**, *115*, 4770–4775.

(19) Tóth, G. An iterative scheme to derive pair potentials from structure factors and its application to liquid mercury. *J. Chem. Phys.* **2003**, *118*, 3949–3955.

(20) Soper, A. K. Tests of the empirical potential structure refinement method and a new method of application to neutron diffraction data on water. *Mol. Phys.* **2001**, *99*, 1503–1516.

(21) Youngs, T. Dissolve: Next generation software for the interrogation of total scattering data by empirical potential generation. *Mol. Phys.* **2019**, *117*, 3464–3477.

(22) Lyubartsev, A.; Mirzoev, A.; Chen, L.; Laaksonen, A. Systematic coarse-graining of molecular models by the Newton inversion method. *Faraday Discuss.* **2010**, *144*, 43–56.

(23) Sun, T.; Minhas, V.; Korolev, N.; Mirzoev, A.; Lyubartsev, A. P.; Nordenskiöld, L. Bottom-up coarse-grained modeling of DNA. *Front. Mol. Biosci.* **2021**, *8*, 645527.

(24) Sun, T.; Minhas, V.; Mirzoev, A.; Korolev, N.; Lyubartsev, A. P.; Nordenskiöld, L. A bottom-up coarse-grained model for nucleosome–nucleosome interactions with explicit ions. *J. Chem. Theory Comput.* **2022**, *18*, 3948–3960.

(25) Shanks, B. L.; Potoff, J. J.; Hoepfner, M. P. Transferable force fields from experimental scattering data with machine learning assisted structure refinement. *J. Phys. Chem. Lett.* **2022**, *13*, 11512–11520.

(26) Deringer, V. L.; Bartók, A. P.; Bernstein, N.; Wilkins, D. M.; Ceriotti, M.; Csányi, G. Gaussian process regression for materials and molecules. *Chem. Rev.* **2021**, *121*, 10073–10141.

(27) Mick, J. R.; Soroush Barhaghi, M.; Jackman, B.; Rushaidat, K.; Schwiebert, L.; Potoff, J. J. Optimized Mie potentials for phase equilibria: Application to noble gases and their mixtures with n-alkanes. *J. Chem. Phys.* **2015**, *143*, 114504.

(28) Soper, A. K. On the uniqueness of structure extracted from diffraction experiments on liquids and glasses. *J. Phys. Condens. Matter* **2007**, *19*, 415108.

(29) Levesque, D.; Verlet, L. Note on X-Ray scattering by argon. *Phys. Rev. Lett.* **1968**, *20*, 905–907.

(30) Angelikopoulos, P.; Papadimitriou, C.; Koumoutsakos, P. Bayesian uncertainty quantification and propagation in molecular dynamics simulations: A high performance computing framework. *J. Chem. Phys.* **2012**, *137*, 144103.

(31) Kulakova, L.; Arampatzis, G.; Angelikopoulos, P.; Chatzidoukas, P.; Papadimitriou, C.; Koumoutsakos, P. Experimental data over quantum mechanics simulations for inferring the repulsive exponent of the Lennard-Jones potential in molecular dynamics. *arXiv* **2017**, arXiv: 1705.08533.

(32) Shanks, B. L.; Sullivan, H. W.; Shazed, A. R.; Hoepfner, M. P. Accelerated Bayesian inference for molecular simulations using local Gaussian process surrogate models. *J. Chem. Theory Comput.* **2024**, *20*, 3798–3808.

(33) Willis, B. T. M.; Carlile, C. J. *Experimental Neutron Scattering*; Oxford University Press, 2017.

(34) Bolmatov, D.; Brazhkin, V. V.; Trachenko, K. Thermodynamic behaviour of supercritical matter. *Nat. Commun.* **2013**, *4*, 2331.

(35) Xu, L.; Kumar, P.; Buldyrev, S. V.; Chen, S.-H.; Poole, P. H.; Sciortino, F.; Stanley, H. E. Relation between the Widom line and the dynamic crossover in systems with a liquid–liquid phase transition. *PNAS* **2005**, *102*, 16558–16562.

(36) Carvalho, R. J. F. L.; Evans, R.; Hoyle, D. C.; Henderson, J. R. The decay of the pair correlation function in simple fluids: Long- versus short-ranged potentials. *J. Phys. Condens. Matter* **1994**, *6*, 9275.

(37) Jovari, P. Neutron diffraction and computer simulation study of liquid CS2 and CSe2. *Mol. Phys.* **1999**, *97*, 1149–1156.

(38) Neuefeind, J.; Feygenson, M.; Carruth, J.; Hoffmann, R.; Chipley, K. K. The nanoscale or-

dered materials diffractometer NOMAD at the spallation neutron source SNS. *Nucl. Instrum. Methods. Phys. Res. B.* **2012**, *287*, 68–75.

(39) Terban, M. W.; Billinge, S. J. L. Structural analysis of molecular materials using the pair distribution function. *Chem. Rev.* **2022**, *122*, 1208–1272.

(40) Motta, M.; Rice, J. E. Emerging quantum computing algorithms for quantum chemistry. *Wiley Interdiscip. Rev. Comput. Mol. Sci.* **2022**, *12*, e1580.

(41) Ratcliff, L. E.; Dawson, W.; Fisicaro, G.; Caliste, D.; Mohr, S.; Degomme, A.; Videau, B.; Cristiglio, V.; Stella, M.; D'Alessandro, M.; Goedecker, S.; Nakajima, T.; Deutsch, T.; Genovese, L. Flexibilities of wavelets as a computational basis set for large-scale electronic structure calculations. *J. Chem. Phys.* **2020**, *152*, 194110.

(42) Duan, C.; Janet, J. P.; Liu, F.; Nandy, A.; Kulik, H. J. Learning from failure: Predicting electronic structure calculation outcomes with machine learning models. *J. Chem. Theory Comput.* **2019**, *15*, 2331–2345.

(43) Rath, Y.; Booth, G. H. Framework for efficient ab initio electronic structure with Gaussian Process States. *Phys. Rev. B* **2023**, *107*, 205119.

(44) Guillot, B.; Mountain, R. D.; Birnbaum, G. Triplet dipoles in the absorption spectra of dense rare gas mixtures. I. Short range interactions. *J. Chem. Phys.* **1989**, *90*, 650–662.

(45) Shell, M. S. The relative entropy is fundamental to multiscale and inverse thermodynamic problems. *J. Chem. Phys.* **2008**, *129*, 144108.

(46) Moore, T. C.; Iacovella, C. R.; McCabe, C. Derivation of coarse-grained potentials via multistate iterative Boltzmann inversion. *J. Chem. Phys.* **2014**, *140*, 224104.

(47) Rudzinski, J. F.; Noid, W. G. A generalized-Yvon-Born-Green method for coarse-grained modeling. Advances, Challenges, and Insight. *European Physical Journal Special Topics* **2015**, *224*, ADS Bibcode: 2015EPJST.224.2193R.

(48) Frommer, F.; Hanke, M. A variational framework for the inverse Henderson problem of statistical mechanics. *Lett. Math. Phys.* **2022**, *112*, 71.

(49) Ivanov, M.; Posysoev, M.; Lyubartsev, A. P. Coarse-Grained Modeling Using Neural Networks Trained on Structural Data. *Journal of Chemical Theory and Computation* **2023**, *19*, 6704–6717, Publisher: American Chemical Society.

(50) Mick, J. R.; Soroush Barhaghi, M.; Jackman, B.; Schwiebert, L.; Potoff, J. J. Optimized Mie potentials for phase equilibria: Application to branched alkanes. *J. Chem. Eng. Data* **2017**, *62*, 1806–1818.

(51) Mie, G. Zur kinetischen Theorie der einatomigen Körper. *Ann. Phys.* **1903**, *316*, 657–697.

(52) Anderson, J. A.; Glaser, J.; Glotzer, S. C. HOOMD-blue: A Python package for high-performance molecular dynamics and hard particle Monte Carlo simulations. *Comput. Mater. Sci.* **2020**, *173*, 109363.

(53) Ramasubramani, V.; Dice, B. D.; Harper, E. S.; Spellings, M. P.; Anderson, J. A.; Glotzer, S. C. freud: A software suite for high throughput analysis of particle simulation data. *Comput. Phys. Commun.* **2020**, *254*, 107275.

(54) Soper, A. Inelasticity corrections for time-of-flight and fixed wavelength neutron diffraction experiments. *Mol. Phys.* **2009**, *107*, 1667–1684.

(55) Barron, A. R. Entropy and the central limit theorem. *Ann. Probab.* **1986**, *14*, 336–342.

(56) Heybrock, S.; Wynen, J.; Vaytet, N. Systematic underestimation of uncertainties by widespread neutron-scattering data-reduction software. *J. Neutron Res.* **2023**, *25*, 65–84.

(57) Yarnell, J. L.; Katz, M. J.; Wenzel, R. G.; Koenig, S. H. Structure factor and radial distribution function for liquid argon at 85K. *Phys. Rev. A* **1973**, *7*, 2130–2144.

(58) Barocchi, F.; Chieux, P.; Magli, R.; Reatto, L.; Tau, M. Neutron diffraction study of liquid krypton and the interatomic interaction. *Phys. Rev. Lett.* **1993**, *70*, 947–950.

(59) Bowron, D. T.; Soper, A. K.; Jones, K.; Ansell, S.; Birch, S.; Norris, J.; Perrott, L.; Riedel, D.; Rhodes, N. J.; Wakefield, S. R.; Botti, A.; Ricci, M.-A.; Grazzi, F.; Zoppi, M. NIMROD: The near and intermediate range order diffractometer of the ISIS second target station. *Review of Scientific Instruments* **2010**, *81*, 033905.

(60) Gelman, A.; Carlin, J. B.; Stern, H. S.; Rubin, D. B. *Bayesian Data Analysis*; Chapman and Hall/CRC, 1995.

(61) Bishop, C. M. *Pattern Recognition and Machine Learning*; Information science and statistics; Springer, 2006.

(62) Foreman-Mackey, D.; Hogg, D. W.; Lang, D.; Goodman, J. emcee: The MCMC Hammer. *Publ. Astron. Soc. Pac.* **2013**, *125*, 306.

(63) Das, K.; Srivastava, A. N. Block-GP: Scalable Gaussian process regression for multimodal data. 2010 IEEE International Conference on Data Mining. 2010; pp 791–796.

(64) Chen, J.; Cao, N.; Low, K. H.; Ouyang, R.; Tan, C. K.; Jaillet, P. Parallel Gaussian process regression with low-rank covariance matrix approximations. 2013; `http://arxiv.org/abs/1305.5826`, arXiv:1305.5826.

(65) Gramacy, R. B.; Apley, D. W. Local Gaussian process approximation for large computer experiments. *J. Comput. Graph. Stat.* **2015**, *24*, 561–578.